QCD crossover temperature and curvature coefficient from unbiased exponential resummation at physical quark masses in (2 + 1)-flavor lattice QCD

Sabarnya Mitra*

Fakultät für Physik, Universität Bielefeld, D-33615 Bielefeld, Germany

(Received 21 August 2026; accepted 13 October 2026; published 30 October 2026)

We present the first application of the unbiased exponential resummation (UER) method to the determination of the QCD pseudocritical temperature T_{pc} at vanishing baryon chemical potential μ_B. By reconstructing the finite-density baryon number susceptibility χ_2^B, we define two thermal-derivative observables whose peak positions yield $T_{pc}^T = 160.2(4)(3)$ MeV and $T_{pc}^C = 158.1(5)(3)$ MeV. We also show that the pseudocritical temperature, T_{pc}^χ obtained from the peak of the fourth-order baryon number susceptibility χ_4^B is consistent with these determinations and with previous lattice-QCD results based on Taylor expansions [1]. Further, we demonstrate that scaling relations [2] between χ_4^B and the thermal derivatives of χ_2^B yield mutually consistent estimates of the leading second order curvature coefficient κ_2^B at the corresponding pseudocritical temperatures. A direct analysis of the μ_B dependence of the pseudocritical temperatures provides an independent but substantially less constrained determination of the curvature, which remains statistically consistent with the scaling-based estimates. These results demonstrate the consistency of this UER method with the expected scaling behavior and establish it as a complementary approach for probing the QCD crossover at small finite baryon density.

DOI: 10.1103/xvsp-mh91

I. INTRODUCTION

Understanding the thermodynamics of strongly interacting matter at nonvanishing temperature and baryon chemical potential μ_B is one of the central goals of finite-density QCD. In particular, determining the location and curvature of the QCD crossover line in the vicinity of $\mu_B = 0$ [3–7] is important for constraining the QCD phase diagram and interpreting heavy-ion collision experiments. Since lattice QCD calculations at finite μ_B are hindered by the sign problem, most first-principles Monte Carlo studies have relied on expansions about $\mu_B = 0$, such as Taylor expansions of thermodynamic observables [8], or on analytic continuation from simulations at imaginary μ_B [9], where the sign problem is absent.

Recently, the framework of unbiased exponential resummation (UER) [10–14] has been developed as an approach for studying finite-density QCD thermodynamics. Its first direct application to the study of Lee-Yang zeros of the QCD partition function at finite isospin density has been demonstrated in Ref. [15]. By exponentiating a Taylor-like expansion truncated at a given order in μ_B, the formalism constructs a finite-density representation of the QCD partition function $\mathcal{Z}$, that reproduces the Taylor expansion exactly up to the truncation order in μ_B remaining in the exponential argument while generating higher-order terms through the exponential structure. This provides a way to reconstruct thermodynamic observables over a finite range of μ_B[1] without explicitly computing all higher-order Taylor coefficients. Previous studies have established and benchmarked this framework for finite-density thermodynamics [10–12], while its application to pseudocritical observables has remained unexplored. In particular, whether the finite-density information reconstructed through unbiased exponential resummation can be used to consistently determine the pseudocritical line at small μ_B including the estimates of T_{pc} and κ_2^B, has not yet been established.

In this paper, we address this question by applying UER to the determination of the QCD pseudocritical line at small baryon chemical potential, with $\mu_Q = \mu_S = 0$,[2] similar to Ref. [1]. Using $(2 + 1)$-flavor lattice QCD simulations with physical quark masses on a $32^3 \times 8$ lattice, we reconstruct the baryon number susceptibility χ_2^B and determine the

*Contact author: smitra@physik.uni-bielefeld.de

Published by the American Physical Society under the terms of the Creative Commons Attribution 4.0 International license. Further distribution of this work must maintain attribution to the author(s) and the published article's title, journal citation, and DOI. Funded by SCOAP³.

[1] In principle, this can be generalized to any chemical potential.

[2] Here, μ_Q and μ_S denote the electric-charge and strangeness chemical potentials, respectively.

pseudocritical temperature from the peak positions of its thermal derivatives. We also estimate the same from the peak of fourth order baryon susceptibility χ_4^B. We further determine the leading-order curvature coefficient κ_2^B using scaling relations involving χ_4^B and the thermal derivatives of χ_2^B, and independently probe the curvature through the explicit μ_B dependence of the pseudocritical temperatures. Throughout this paper, we denote $\hat{\mu}_B \equiv \mu_B/T$.

II. UER AND LATTICE SETUP

A. Formalism in brief

The method of UER [10–12] provides a representation of the ratio, R_N of $\mathcal{Z}$ at finite $\hat{\mu}_B$ to $\mathcal{Z}$ at zero $\hat{\mu}_B$ truncated to N^{th} order in $\hat{\mu}_B$, by means of an average over a gauge ensemble simulated at $\hat{\mu}_B = 0$,

$$R_N = \frac{\mathcal{Z}_N(\hat{\mu}_B)}{\mathcal{Z}(0)} = \left\langle \exp\left[\sum_{n=1}^{N} \frac{\bar{D}_n}{n!}\hat{\mu}_B^n\right]\right\rangle. \tag{1}$$

Here, $\bar{D}_n$ is the nth order $\hat{\mu}_B$ derivative of the logarithm of the fermion determinant at $\hat{\mu}_B = 0$. This includes the correction terms [11] required to ensure the unbiased nature of the exponential resummation procedure. At a finite temperature T, the excess pressure $\hat{P} = \Delta P/T^4$, number density $\hat{\mathcal{N}} = \mathcal{N}/T^3$, baryon number susceptibility $\hat{\chi}_2^B = \chi_2^B/T^2$ to $\mathcal{O}(\hat{\mu}_B^N)$ are given by

$$\hat{P}_N = \frac{\ln R_N}{VT^3}, \qquad \hat{\mathcal{N}}_N = \frac{\partial \hat{P}_N}{\partial \hat{\mu}_B}, \qquad \hat{\chi}_{2,N}^B = \frac{\partial^2 \hat{P}_N}{\partial \hat{\mu}_B^2}, \tag{2}$$

where V is the system volume. In this paper, we apply this formalism using $N = 4$ and evaluate $\hat{\chi}_{2,4}^B$ in Eq. (2) derived from the stochastic estimate of R_4 obtained here using bootstrap sampling. This reproduces the Taylor expansion up to $\mathcal{O}(\hat{\mu}_B^2)$ with correction terms appearing from $\mathcal{O}(\hat{\mu}_B^4)$ onward. Subsequent statistical uncertainties are obtained taking into account the correlation terms appearing in the covariance matrix. With the data points of $\hat{\chi}_{2,4}^B$ as function of T, we proceed on determining the estimates of $\mathrm{T_{pc}}$ and κ_2^B in this paper. A comparative study of these estimates obtained from $N = 2$ and $N = 4$ of UER is provided in Appendix B. For simplicity, we denote $\hat{\chi}_{2,4}^B$ as $\hat{\chi}_2^B$ from here on.

B. Lattice setup

We perform $(2+1)$-flavor lattice QCD simulations using the highly improved staggered quark (HISQ) action with physical light and strange-quark masses on $32^3 \times 8$ lattices over the temperature range $T \in [135\text{:}176]$ MeV, with $\mathcal{O}(10^5$–$10^6)$ gauge configurations at each temperature. Along with the HISQ action, we consider the $\mathcal{O}(a^2)$ improved Symanzik gauge action [16] together which constitute the QCD action, S_{QCD}.[3] The scale setting of this work determining the different input T values of the $\hat{\chi}_2$ data points, is based on the line of constant physics (LCP) given in Ref. [5]. The ratio R_4 is evaluated using the full configuration ensemble at each temperature, with bootstrap sampling employed to estimate the statistical uncertainties. Using this setup and the same bootstrap sampling framework, we likewise estimate $\mathrm{T_{pc}}$ and κ_2^B, along with associated uncertainties of these observables.

III. COMPARISON WITH PADÉ RESULTS

Prior to discussing our main results of pseudocritical temperature and curvature coefficient estimates evaluated using UER, it is important to review and recheck the reliability of these resummation results of bulk thermodynamic observables. Although done before in the context of Taylor series expansion in Ref. [11], we show this here by comparing these results with similar results derived from Padé resummation [1].

We present this comparison in Fig. 1, where the second and fourth order unbiased resummation results for excess pressure $\hat{P}$, and number density $\hat{\mathcal{N}}$ are outlined alongside similar and higher order Padé results as function of $\hat{\mu}_B$, for $T = 135$, 157 and 176 MeV. While we use Padé [2, 2] and [4, 4] results for $\hat{P}$, their spline $\hat{\mu}_B$-derivatives are considered as similar Padé estimates for $\hat{\mathcal{N}}$. Almost two orders of higher statistics as compared to Ref. [11] have been used for these new UER results. Besides having agreement between $N = 2$ and $N = 4$ UER results of $\hat{P}$ and $\hat{\mathcal{N}}$ in this $\hat{\mu}_B$ range, equally apparent from this figure, is the promising consistency between these two resummation procedures. These results are also well-consistent with similar order Taylor series values shown here in Fig. 1. In this section, we have restricted this discussion and associated comparative analysis for $\hat{\mu}_B \in$ [0: 1.2] only. This is adequate enough to support the reliability of UER results needed and relevant for this work, where the central estimates of $\mathrm{T_{pc}}$ and κ_2^B are evaluated by making use of these UER results in small $\hat{\mu}_B$ regime, $\hat{\mu}_B \leq 0.5$ only. A further study in higher baryon density along this direction for more temperatures, is reserved for a future work.

IV. PSEUDOCRITICAL TEMPERATURE

An important purpose of this work, as discussed before is determination of pseudocritical temperature $\mathrm{T_{pc}}$ from UER. This is done by studying the temperature dependence of the baryon number susceptibility, $\hat{\chi}_2^B$, and subsequently considering its temperature derivative. As already argued in Ref. [2], the temperature derivative of $\hat{\chi}_2^B$ develops a finite pronounced peak at the chiral transition temperature T_c in

[3]This QCD action S_{QCD} enters as Boltzmann weight in QCD partition function integral, $Z = \int DU \exp(-S_{\text{QCD}})$.

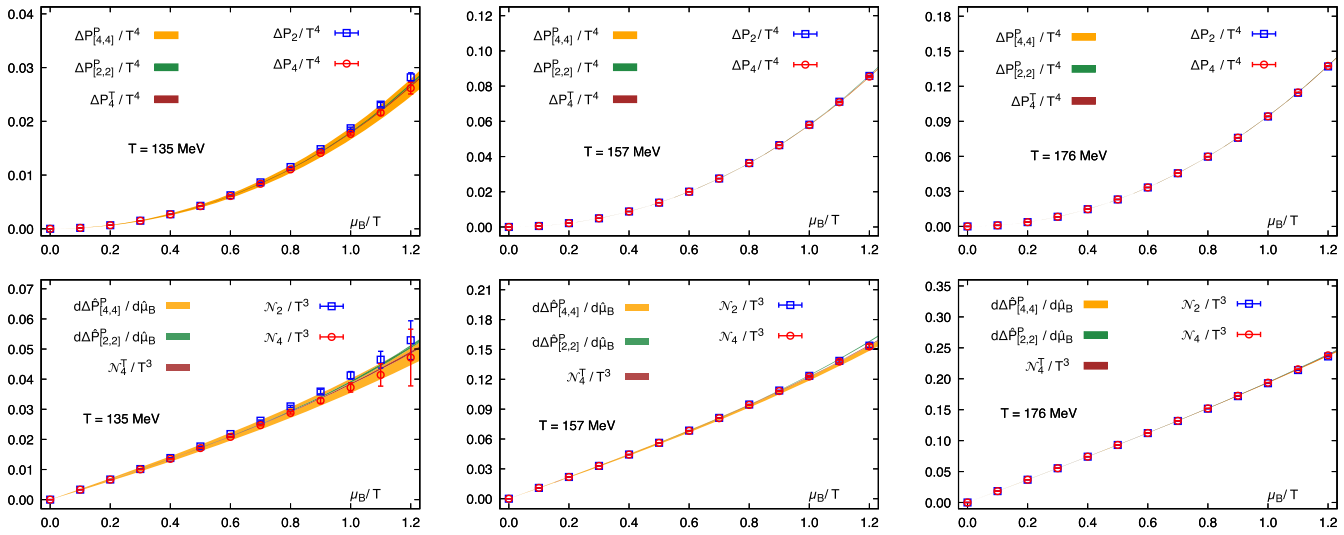


FIG. 1. Comparison of results between UER (blue and red points) and same obtained from Padé resummation (orange and green bands) and Taylor expansion results (brown bands) for excess pressure $\Delta\hat{P}_4$ (top) and number density $\hat{\mathcal{N}}_3$ (bottom), where direct derivative results $\partial\hat{P}^P_{[2,2]}/\partial\hat{\mu}_B$ are also presented (magenta bands).

the chiral limit, which broadens away from this limit. At physical quark masses, this broadened peak therefore provides an estimator of the pseudocritical temperature T_{pc}. We therefore estimate T_{pc} from the peak positions of two such corresponding derivative observables at physical light-quark masses, at vanishing $\hat{\mu}_B$, as discussed in the following sections.

A. From χ_2 analysis

The temperature dependence of the baryon number susceptibility, $\hat{\chi}^B_2$, obtained using the unbiased exponential resummation framework on $N_\tau = 8$ lattices, is shown in Fig. 2 for six values of $\hat{\mu}_B$, $\hat{\mu}_B \in [0{:}0.5]$. We construct smooth cubic splines to interpolate the resummed data points of $\hat{\chi}^B_2$ as a function of temperature. We then subsequently construct two thermal derivative observables

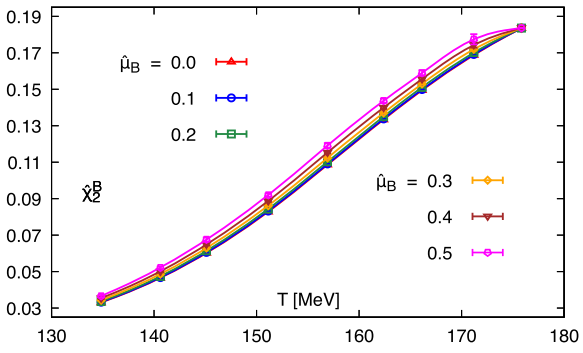


FIG. 2. The baryon number susceptibility, $\hat{\chi}^B_2$ obtained using UER on $N_\tau = 8$ lattices, shown as a function of T, for $0 \le \hat{\mu}_B \le 0.5$. Six different colors are used for the six values of $\hat{\mu}_B$. (More details in text).

$$\hat{\chi}_T = T\frac{\partial\hat{\chi}^B_2}{\partial T}, \qquad \hat{\chi}_C = T_c\frac{\partial\hat{\chi}^B_2}{\partial T}, \tag{3}$$

whose maxima define the corresponding estimates T^T_{pc} and T^C_{pc} of the pseudocritical temperature T_{pc} at $\hat{\mu}_B = 0$.

For the definition of $\hat{\chi}_C$ in Eq. (3), we take $T_c = 145$ MeV [17–20]. As discussed above, T_{pc} approaches T_c in the vanishing light-quark-mass limit, consistent with the expected universal scaling behavior of the chiral transition [21]. The corresponding observables $\hat{\chi}_T$ and $\hat{\chi}_C$, shown in Fig. 3, are obtained analytically as functions of T from the spline interpolation. The interpolation range is restricted to $[135{:}172]$ MeV, which encompasses the crossover region while avoiding poorly constrained extrapolation of the constructed cubic splines.

Figure 3 illustrates that both $\hat{\chi}_T$ and $\hat{\chi}_C$ exhibit clear peak structures as functions of T. Consistent with Ref. [2], we find that the peak positions shift toward lower temperatures, while the corresponding peak heights increase with increasing $\hat{\mu}_B$ although, the latter increase is incremental over this range of $\hat{\mu}_B$ considered. At $\hat{\mu}_B = 0$, the peak positions of these two observables yield

$$T^T_{pc} = 160.2(4)(2)\ \text{MeV}, \qquad T^C_{pc} = 158.1(5)(3)\ \text{MeV}, \tag{4}$$

where the first and second uncertainties denote statistical and systematic errors, respectively. The difference between T^T_{pc} and T^C_{pc} is consistent with the expected observable dependence of the crossover temperature at physical quark masses. Although the same thermal derivatives exhibit well-defined peaks also at finite $\hat{\mu}_B$, their interpretation as estimators of the finite-density pseudocritical line

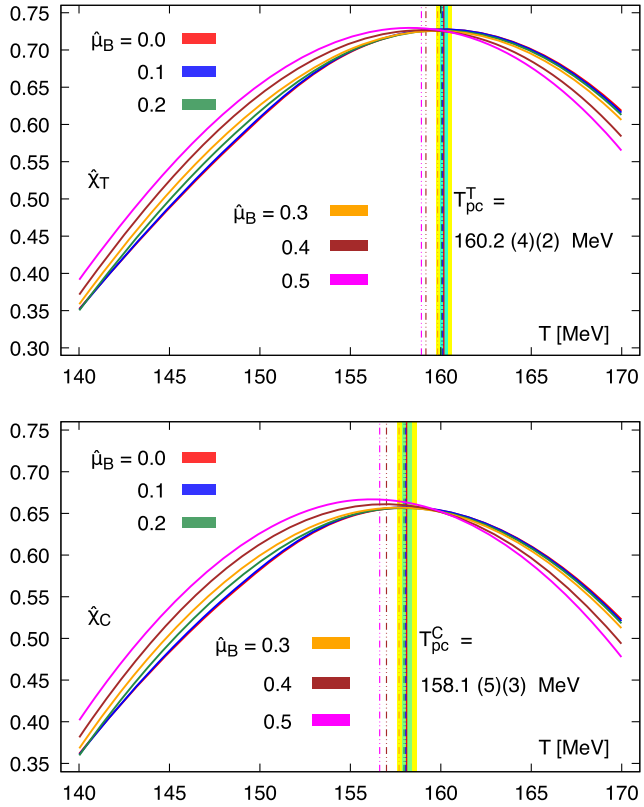


FIG. 3. Top: the thermal derivative, $\hat{\chi}_T$ [Eq. (3)] vs T shown for the same six $\hat{\mu}_B$ values as in Fig. 2, following the same color convention. Bottom: the corresponding result for $\hat{\chi}_C$ [Eq. (3)]. The peak positions for nonvanishing $\hat{\mu}_B$ are indicated by vertical dotted lines, with similar color convention. The red solid line gives the same for $\hat{\mu}_B = 0$, thereby giving estimates of T^T_{pc}, T^C_{pc}. The yellow (cyan) bands show the statistical (systematic) errors on respective T_{pc} values.

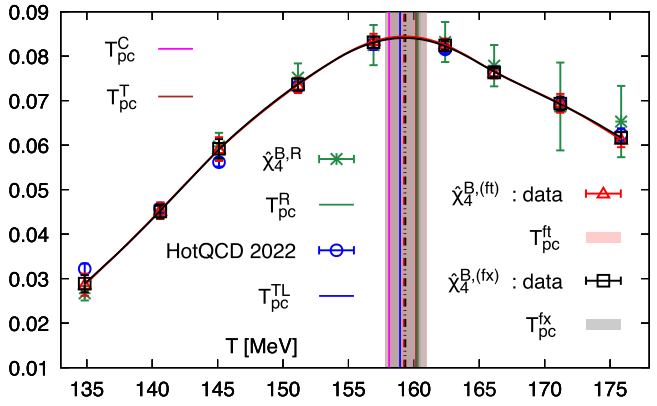


FIG. 4. $\hat{\chi}_4^B$ calculated from Eq. (5) shown as a function of T using *i)* $\hat{\chi}_2^B(0)$ directly from the resummed data (red triangles) and *ii)* treating $\hat{\chi}_2^B(0)$ as a fit parameter (black squares). The red and black bands outline T^{ft}_{pc} and T^{fx}_{pc} with errors. The magenta and brown solid lines highlight T^C_{pc} and T^T_{pc}. The green and blue points (lines) outline $\hat{\chi}_4^B$ (T^R_{pc}) obtained from directly resummed result and HotQCD Taylor analyses (T^{TL}_{pc}) [1], respectively.

requires a dedicated analysis of the underlying universal scaling behavior. We therefore restrict the present determination of T_{pc} to $\hat{\mu}_B = 0$ and leave a detailed finite-density analysis of possible pseudocritical temperature estimates for future work.

B. From χ_4 analysis

We further explore the temperature dependence of the fourth-order baryon number susceptibility, $\hat{\chi}_4^B$, as a complementary estimator of T_{pc} at $\hat{\mu}_B = 0$. As the second derivative of $\hat{\chi}_2^B$ with respect to $\hat{\mu}_B$, $\hat{\chi}_4^B = \partial^2\hat{\chi}_2^B/\partial\hat{\mu}_B^2$ at $\hat{\mu}_B = 0$ exhibits a pronounced peak in the crossover region, providing a similar determination of the pseudocritical temperature T_{pc}. Like the thermal derivative observables $\hat{\chi}_T$ and $\hat{\chi}_C$, the interpretation of the peak of $\hat{\chi}_4^B$ at finite $\hat{\mu}_B$ involves additional higher-order derivatives of the universal scaling functions and is therefore beyond the scope of the present analysis.

We obtain $\hat{\chi}_4^B(T)$ at $\hat{\mu}_B = 0$ from the $\hat{\mu}_B$ dependence of the resummed $\hat{\chi}_2^B$ at each temperature,

$$\hat{\chi}_2^B(\hat{\mu}_B) = \hat{\chi}_2^B(0) + \frac{\hat{\mu}_B^2}{2!}\hat{\chi}_4^B(0) + \mathcal{O}(\hat{\mu}_B^4). \tag{5}$$

The resulting $\hat{\chi}_4^B(T)$ is shown in Fig. 4, where it exhibits good agreement with the corresponding Taylor-expansion results produced by HotQCD collaboration [1], shown as blue points for each temperature in this figure. The peak positions of our $\hat{\chi}_4^{B,(ft)}$ and $\hat{\chi}_4^{B,(fx)}$ estimates yield

$$T^{ft}_{pc} = 159.4(10)(12)\ \text{MeV}, \qquad T^{fx}_{pc} = 159.4(9)(8)\ \text{MeV}. \tag{6}$$

In the "ft" determination, $\hat{\chi}_2^B(0)$ is treated as a fit parameter simultaneously together with $\hat{\chi}_4^B(0)$ whereas in the "fx" determination, $\hat{\chi}_2^B(0)$ is fixed to its directly reconstructed resummed value, for each temperature.

We show these results in Fig. 4, in which we find that both determinations in Eq. (6) are consistent with each other and exhibit good agreement with the pseudocritical temperature estimates T^T_{pc} and T^C_{pc} obtained from the thermal derivative observables $\hat{\chi}_T$ and $\hat{\chi}_C$ in Eq. (4), as shown in Fig. 3. We additionally evaluate $\hat{\chi}_4^B$ directly within the UER framework, and show the first result, $\hat{\chi}_4^{B,R}$ from this setup in Fig. 4. This observable, at $\hat{\mu}_B = 0$, shows consistent behavior with other results and yields

$$T^R_{pc} = 160.3(40)(13)\ \text{MeV}. \tag{7}$$

The larger statistical uncertainty reflects the enhanced noise and correlations associated with the direct computation of a higher-order observable, within the bootstrap analysis of the UER framework. A detailed study of its statistical and

systematic uncertainties is left for future work. For comparison, the maximum of $\hat{\chi}_4^B$ obtained from the Taylor-expansion analysis [1] using the same interpolating procedure, gives a consistent estimate

$$T_{pc}^{TL} = 158.9(10)(14)\ \text{MeV}. \tag{8}$$

V. CURVATURE COEFFICIENT

A. Scaling estimate

At $\hat{\mu}_B = 0$, the leading-order curvature coefficient κ_2^B can be extracted from ratios of the singular contributions to the relevant observables, as demonstrated in Ref. [2]. Since our analysis is performed within the scaling regime, we neglect the subleading nonsingular contributions. In the resulting ratios, the nonuniversal scaling parameters and the corresponding derivatives of the free-energy scaling function $f_f(z)$ cancel, allowing the curvature coefficient to be expressed directly in terms of the susceptibilities. We consider the following estimator for curvature

$$\kappa_{2,\text{sc}}^B = \frac{1}{6}\frac{\hat{\chi}_4^B}{\hat{\chi}_C}, \tag{9}$$

derived from the scaling relations, where $\hat{\chi}_C = T_c d\hat{\chi}_2^B/dT$ is the corresponding thermal derivative introduced above. One can also obtain this value from $\hat{\chi}_T$, using the identity $\hat{\chi}_T = T\hat{\chi}_C/T_c$.

We evaluate this curvature estimator using the two determinations of $\hat{\chi}_4^B$ discussed above: (i) the result obtained by treating $\hat{\chi}_2^B$ as a fit parameter, denoted by (ft), and (ii) the result obtained with $\hat{\chi}_2^B$ fixed directly from the resummed data, denoted by (fx). The resulting values of $\kappa_{2,\text{sc}}^{B,T} = \kappa_{2,\text{sc}}^B(T_{pc}^T)$ and $\kappa_{2,\text{sc}}^{B,C} = \kappa_{2,\text{sc}}^B(T_{pc}^C)$, evaluated at the pseudocritical temperature estimates T_{pc}^T and T_{pc}^C determined from the corresponding thermal derivatives, are summarized in Table I.

For $T = T_{pc}^T = 160.2$ MeV, we obtain 0.02082(18) and 0.02083(17) using the $\hat{\chi}_4^{B,(\text{ft})}$ and $\hat{\chi}_4^{B,(\text{fx})}$ determinations, respectively. The corresponding $\kappa_{2,\text{sc}}^{B,T}$ and $\kappa_{2,\text{sc}}^{B,C}$ estimates agree within the quoted precision. At $T = T_{pc}^C = 158.1$ MeV, the corresponding values are 0.02062(22) and 0.02066(21). Thus, the agreement between the values of the κ_2^B estimates in (ft) and (fx) determinations provides an additional consistency check on the scaling analysis.

TABLE I. Comparison of the second order curvature estimate, κ_2^B, at the two pseudocritical temperatures, $T_{pc}^T = 160.2$ MeV and $T_{pc}^C = 158.1$ MeV, as mentioned in Eq. (4).

Curvature	$\kappa_{2,\text{sc}}^B(T_{pc}^T)$	$\kappa_{2,\text{sc}}^B(T_{pc}^C)$
$\hat{\chi}_4^{B,(\text{ft})}$	0.02082(18)	0.02062(22)
$\hat{\chi}_4^{B,(\text{fx})}$	0.02083(17)	0.02066(21)

TABLE II. Curvature estimate κ_2^B at $T_{pc}^\chi = 159.4$ MeV, as obtained from the peak position of $\hat{\chi}_4^B$ in T [Eq. (6)].

Curvature	$\kappa_{2,\text{sc}}^B(T_{pc}^\chi)$
$\hat{\chi}_4^{B,(\text{ft})}$	0.02073(20)
$\hat{\chi}_4^{B,(\text{fx})}$	0.02076(18)

Averaging the corresponding estimates at each pseudocritical temperature using bootstrap analysis on each of the working 2000 bootstrap samples gives

$$\kappa_{2,\text{sc}}^{B,T} = 0.02082(14), \qquad \kappa_{2,\text{sc}}^{B,C} = 0.02064(15). \tag{10}$$

These values are consistent with the curvature obtained at comparable temperatures from Taylor expansion methods [2]. Their small difference is also consistent with the quoted uncertainties, indicating that the scaling-based curvature estimate is stable over the range of pseudocritical temperatures considered here.

We further perform the same analysis at $T = T_{pc}^\chi = 159.4$ MeV where, T_{pc}^χ [4] is determined from the peak position of $\hat{\chi}_4^B$ as a function of temperature. The corresponding curvature estimates are shown in Table II. The values obtained from $\kappa_2^{B,T}$ and $\kappa_2^{B,C}$, as well as those from the (ft) and (fx) determinations, are again consistent. Averaging these estimates gives

$$\kappa_{2,\text{sc}}^B(T_{pc}^\chi) = 0.02075(14). \tag{11}$$

All central values and uncertainties quoted in Eqs. (10) and (11) are obtained from bootstrap analysis. The correlations among these derived observables are taken into account through the bootstrap analysis. All quantities are evaluated on the same bootstrap samples, such that their statistical correlations are retained when forming temperature derivatives, ratios, and pseudocritical temperature as well as curvature coefficient estimates. In particular, $\hat{\chi}_T$ and $\hat{\chi}_C$ are obtained from the temperature dependence of $\hat{\chi}_2^B$ within each bootstrap sample, while the curvature estimates involving $\hat{\chi}_4^B/\hat{\chi}_T$ and $\hat{\chi}_4^B/\hat{\chi}_C$ are likewise evaluated on each bootstrap sample before determining the statistical distribution of the resulting quantity. Thus, the quoted uncertainties include and do take into account, the correlations between the underlying observables rather than treating their statistical fluctuations as independent.

When taken together along with this error analysis, we observe the three estimates $\kappa_{2,\text{sc}}^B(T_{pc}^T)$, $\kappa_{2,\text{sc}}^B(T_{pc}^C)$, and

[4] Here, T_{pc}^χ is obtained as the bootstrap average of (ft) and (fx) determinations introduced before.

$\kappa^B_{2,\mathrm{sc}}(\mathrm{T}^{\chi}_{\mathrm{pc}})$, as presented in Eqs. (10) and (11) are mutually consistent. This demonstrates the stability of $\kappa^B_{2,\mathrm{sc}}$, the scaling-based curvature estimate of κ^B_2 with respect to the choice of pseudocritical temperature estimator.

B. From pseudocritical line analysis

Next, we estimate κ^B_2 from the $\hat{\mu}_B$ dependence of the pseudocritical temperatures $\mathrm{T}^T_{\mathrm{pc}}$ and $\mathrm{T}^C_{\mathrm{pc}}$, determined from the peak positions of $\hat{\chi}_T$ and $\hat{\chi}_C$, respectively, as discussed in the previous section.

At vanishing baryon chemical potential, $\hat{\mu}_B = 0$, we determine the pseudocritical temperatures T^T_{pc} and T^C_{pc} from the peak positions of the thermal derivatives $\hat{\chi}_T = Td\hat{\chi}^B_2/dT$ and $\hat{\chi}_C = T_c d\hat{\chi}^B_2/dT$ respectively. This construction is motivated by the scaling behavior of $\hat{\chi}^B_2$, which is an energylike observable. While these observables $\hat{\chi}_T$ and $\hat{\chi}_C$ develop a cusp at chiral phase transition temperature T_c in the chiral limit, this cusp gets smoothed into a finite broad peak for physical quark masses at pseudocritical temperatures $\mathrm{T}^T_{\mathrm{pc}}$ and $\mathrm{T}^C_{\mathrm{pc}}$. In the chiral limit, this cusp corresponds to the nonanalytic singular behavior of chiral phase transition, which is a genuine phase transition [1]. This nonanalytic singular form of temperature dependence in the chiral limit gets smoothed into an analytic, finite maximum in its thermal derivative in the crossover region, away from the chiral limit. Since different observables generally attain their maxima at different temperatures in a crossover, the peak positions of these derivative-based estimators define observable-dependent T_{pc} values, at $\hat{\mu}_B = 0$.

At finite nonzero μ_B, however this correspondence between the peak position of these estimators and the pseudocritical temperature estimates defined from the underlying universal scaling condition is not exact. In scaling terms, the leading singular temperature dependence of $\hat{\chi}^B_2$ at $\hat{\mu}_B = 0$ is governed entirely by the first derivative of the free-energy scaling function, $f'_f(z)$. At finite $\hat{\mu}_B$ in contrast, an explicit chemical-potential dependence of the scaling variable enters in this relation, which generates additional contributions involving higher derivatives of the scaling function. Schematically up to $\mathcal{O}(\hat{\mu}^2_B)$, the singular part of $\hat{\chi}^B_2$, $\hat{\chi}^{B,s}_2$ can be written as

$$\hat{\chi}^{B,s}_2(\hat{\mu}_B) \propto [f'_f(z(T,\mu_B)) + K\,\hat{\mu}^2_B\, f''_f(z(T,\mu_B))], \qquad (12)$$

where K is a positive nonvanishing proportionality factor containing the corresponding nonuniversal scaling factors. Consequently taking a thermal derivative of $\hat{\chi}^{B,s}_2(\hat{\mu}_B)$ generates contributions involving f''_f as well as leading higher order terms proportional to $\hat{\mu}^2_B f'''_f$, which vanishes at $\hat{\mu}_B = 0$. Thus at finite $\hat{\mu}_B$, the peak of the thermal derivative of χ^B_2 does not in general, coincide exactly with the pseudocritical temperature defined by the underlying scaling condition. A naive quantitative extent of this approximation is briefed in Appendix A.

We therefore refer to the peak positions of χ_T and χ_C at finite μ_B as susceptibility-based pseudocritical proxies, rather than identifying them exactly with the pseudocritical line. The distinction can become increasingly relevant with increasing $\hat{\mu}_B$, as higher-order finite-density contributions to the scaling observables become more important. However as detailed in Appendix A, this deviation is small within the restricted range $\hat{\mu}_B \in [0\text{: }0.5]$ considered here for curvature extraction. In this context therefore, this allows us to use them as operational estimators of $\mathrm{T}^T_{\mathrm{pc}}$ and $\mathrm{T}^C_{\mathrm{pc}}$ in this section, and extract the corresponding curvature coefficients from respective fit analysis. For $x = T$, C, we parametrize the pseudocritical line as

$$\mathrm{T}^x_{\mathrm{pc}}(\hat{\mu}_B) = \mathrm{T}^x_{\mathrm{pc}}(0)[1 - \kappa^{B,x}_{2,\mathrm{pc}}\hat{\mu}^2_B + \mathcal{O}(\hat{\mu}^4_B)], \qquad (13)$$

where, we denote $\kappa^{B,x}_{2,\mathrm{pc}} \equiv \kappa^B_{2,\mathrm{pc}}(\mathrm{T}^x_{\mathrm{pc}})$ as the curvature estimate obtained from pseudocritical line in this section. We fit the $\hat{\mu}_B$-dependent peak positions to this form over the range $0 \le \hat{\mu}_B \le 0.5$, obtaining

$$\kappa^{B,T}_{2,\mathrm{pc}} = 0.029(32), \qquad \kappa^{B,C}_{2,\mathrm{pc}} = 0.033(27), \qquad (14)$$

using only $\kappa^{B,T}_{2,\mathrm{pc}}$ and $\kappa^{B,C}_{2,\mathrm{pc}}$ as fit parameters in our fitting procedure. The solid black and blue curves outline the direct fit results of $\mathrm{T}^T_{\mathrm{pc}}(\hat{\mu}_B)$ and $\mathrm{T}^C_{\mathrm{pc}}(\hat{\mu}_B)$ of Eq. (13), while the dotted curves use instead the κ^B_2 estimates of scaling relations, Eq. (10). This comparison is illustrated in Fig. 5, where we show only upto $\hat{\mu}_B = 0.3$ for visual representation. The solid black and blue curves show the direct fits to the $\mathrm{T}^T_{\mathrm{pc}}(\hat{\mu}_B)$ and $\mathrm{T}^C_{\mathrm{pc}}(\hat{\mu}_B)$ data using Eq. (13), with only the $\kappa^{B,T}_2$ and $\kappa^{B,C}_2$ as the fit parameters. The dotted curves, $\mathrm{T}^{T,\mathrm{sc}}_{\mathrm{pc}}(\hat{\mu}_B)$ and $\mathrm{T}^{C,\mathrm{sc}}_{\mathrm{pc}}(\hat{\mu}_B)$ instead use the corresponding $\mathrm{T}^T_{\mathrm{pc}}(0)$ and $\mathrm{T}^C_{\mathrm{pc}}(0)$ values from Eq. (4), together with the

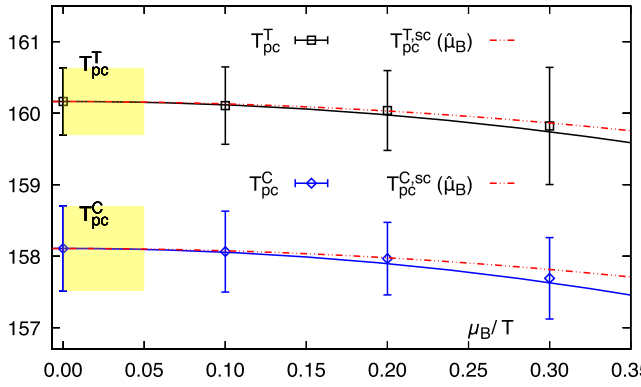


FIG. 5. Estimates of $\kappa^{B,T}_{2,\mathrm{pc}}$ and $\kappa^{B,C}_{2,\mathrm{pc}}$ (see text for details) obtained from pseudocritical line analysis, using the parametrization of $\mathrm{T}_{\mathrm{pc}}(\hat{\mu}_B)$ in Eq. (13). The yellow bands represent respective errors on $\mathrm{T}^T_{\mathrm{pc}}$ and $\mathrm{T}^C_{\mathrm{pc}}$ at $\hat{\mu}_B = 0$. (Details in text).

TABLE III. Dependence of the curvature coefficients extracted from the pseudocritical line on the maximum value of $\hat{\mu}_B$ included in the fit. The pseudocritical temperatures are obtained using the cubic-spline interpolation over $135 \leq T \leq 172$ MeV, over the full range $0 \leq \hat{\mu}_B \leq 0.5$.

$\hat{\mu}_B^{\max}$	$\kappa_{2,\mathrm{pc}}^T$	$\kappa_{2,\mathrm{pc}}^C$
0.1	0.036(317)	0.028(320)
0.2	0.021(80)	0.023 (76)
0.3	0.023(46)	0.028 (35)
0.4	0.029(36)	0.033(29)
0.5	0.029(32)	0.033(27)

curvature estimates obtained from the $\hat{\mu}_B = 0$ scaling relations in Eq. (10).

As shown in this figure, the two sets of curves are statistically consistent within the uncertainties of the pseudocritical line analysis. The central values of the curvature coefficients obtained from the direct analysis of the pseudocritical line in Eq. (14) are also found to be relatively close to the corresponding estimates from the scaling relations in Eq. (10). The direct determination, however, remains less precisely constrained, as reflected by the comparatively large uncertainties on both $\kappa_{2,\mathrm{pc}}^{B,T}$ and $\kappa_{2,\mathrm{pc}}^{B,C}$. Thus, within the present precision, the two approaches yield mutually consistent estimates of the curvature.

The sensitivity of this direct determination of κ_2^B to the fitting range, $\hat{\mu}_B \in [0\colon \hat{\mu}_B^{\max}]$ is further illustrated in Table III, where we show the extracted curvature coefficients, $\kappa_{2,\mathrm{pc}}^T$ and $\kappa_{2,\mathrm{pc}}^C$ for different values of the maximum chemical potential, $\hat{\mu}_B^{\max}$. In either case, we find the uncertainties decrease substantially as the fitting range is extended from $\hat{\mu}_B^{\max} = 0.2$ to 0.3, while the central values remain mutually consistent within the corresponding uncertainties. For $\hat{\mu}_B^{\max} > 0.3$, the extracted curvature coefficients show comparatively mild variations, with a further reduction of the uncertainties upon extending the range to $\hat{\mu}_B^{\max} = 0.5$. This behavior reflects the finite-$\hat{\mu}_B$ nature of the pseudocritical line analysis in which, a sufficiently large $\hat{\mu}_B$ lever arm is required to constrain the quadratic dependence, while the statistical fluctuations of the individual $T_{\mathrm{pc}}(\hat{\mu}_B)$ determinations propagate into the global fit. The choice, $\hat{\mu}_B^{\max} = 0.5$ therefore provides a substantially more precise determination while remaining consistent with the results obtained from the smaller fitting ranges.

In contrast, the scaling determination does not require a finite-μ_B fit and instead provide a local determination of the curvature from the observables and their temperature derivatives evaluated at $\mu_B = 0$, resulting in smaller statistical uncertainties. Thus, although both approaches use the same underlying lattice data and determine the same physical curvature, they extract κ_2^B through statistically different estimators. This comparison provides therefore a correlated internal cross-check of the curvature coefficient κ_2^B using two complementary analyses based on shared ensembles. The scaling-relation analysis determines κ_2^B entirely from $\hat{\mu}_B = 0$ susceptibilities, following Ref. [2], whereas the pseudocritical line analysis probes the explicit $\hat{\mu}_B$ dependence of the pseudocritical temperatures $\mathrm{T}_{\mathrm{pc}}(\hat{\mu}_B)$. The statistical compatibility of the two determinations, despite the substantially larger uncertainty and less-constrained nature of the direct determination, supports the consistency of the curvature extracted from the scaling analysis. This comparison is also consistent with the use of the finite-volume-corrected value $T_c = 145$ MeV [17–20] in the scaling analysis.

VI. CONCLUSIONS AND OUTLOOK

In this paper, we have applied the UER framework to the determination of the QCD crossover line at finite baryon chemical potential $\hat{\mu}_B$. Using $(2+1)$-flavor lattice QCD simulations with physical quark masses on a $32^3 \times 8$ lattice, we reconstruct the baryon number susceptibility $\hat{\chi}_2^B$ and determine the pseudocritical temperature T_{pc} from the maxima of its thermal derivatives $\hat{\chi}_T$ and $\hat{\chi}_C$ as functions of T. We determine the leading curvature coefficient κ_2^B using two distinct approaches: (i) a direct analysis of the pseudocritical line and (ii) scaling relations evaluated at $\hat{\mu}_B = 0$. From the $\hat{\mu}_B$ dependence of the pseudocritical temperatures defined from the peaks of $\hat{\chi}_T$ and $\hat{\chi}_C$, we obtain

$$\kappa_{2,\mathrm{pc}}^{B,T} = 0.029(32), \qquad \kappa_{2,\mathrm{pc}}^{B,C} = 0.033(27).$$

These direct determinations are substantially less constrained than the corresponding estimates obtained from the scaling relations, but remain consistent with them within the statistical uncertainties. The scaling-based analysis gives

$$\begin{aligned}\kappa_{2,\mathrm{sc}}^B(\mathrm{T}_{\mathrm{pc}}^T) &= 0.02082(14),\\ \kappa_{2,\mathrm{sc}}^B(\mathrm{T}_{\mathrm{pc}}^C) &= 0.02064(15),\\ \kappa_{2,\mathrm{sc}}^B(\mathrm{T}_{\mathrm{pc}}^\chi) &= 0.02075(14),\end{aligned}$$

where $\mathrm{T}_{\mathrm{pc}}^\chi$ is determined from the peak position of the fourth-order baryon number susceptibility $\hat{\chi}_4^B$. The scaling-based curvature estimates are obtained from ratios involving $\hat{\chi}_4^B$ and the thermal derivatives of $\hat{\chi}_2^B$, for which the nonuniversal scaling parameters cancel in the scaling regime. Even though the former outlines estimates of κ_2^B, $\kappa_{2,\mathrm{pc}}^T$ and $\kappa_{2,\mathrm{pc}}^C$ that are less constrained along with relatively larger uncertainties, the consistency of these estimates with the same derived from scaling relations, $\kappa_{2,\mathrm{sc}}^{B,T}$ and $\kappa_{2,\mathrm{sc}}^{B,C}$ provides a nontrivial cross-check of the resummed description, as well as of these two complementary approaches of determining κ_2^B.

Within the present analysis, we have explicitly investigated the dependence of the pseudocritical temperatures,

T_{pc}^{T} and T_{pc}^{C} on the order of truncation in UER, interpolating functional form, temperature interpolation in form of numerical resolution of the cubic spline fit procedure as well as also on the range of temperature utilized for fitting the data points. As vividly illustrated in Appendix B, these arguments are presented to validate our choice of the parameters of fitting considered for this work and the analysis. Statistical correlations among derived observables are retained through the bootstrap procedure, with quantities entering derived estimators are evaluated on the same bootstrap samples before forming ratios, derivatives, or pseudocritical quantities. Thus, the quoted statistical uncertainties do account for the correlations among the underlying observables rather than treating them as statistically independent. In particular, the UER approach independently reconstructs the finite-density susceptibility and its associated thermal derivatives, while the resulting observables satisfy the scaling relations for the curvature underlying corresponding Taylor-expansion analyses. This demonstrates consistency of the resummation framework with previous lattice QCD determinations based on Taylor expansions. The present results demonstrate that UER can be extended beyond bulk thermodynamic observables to probe the location and curvature of the QCD crossover line at finite density. Together with our previous studies of the resummed equation of state [10–14] and Lee-Yang zeros [15], this work establishes the framework as a complementary approach for investigating finite-density QCD in the vicinity of $\hat{\mu}_B = 0$.

The present analysis is performed on $32^3 \times 8$ lattices, corresponding to an aspect ratio $N_s/N_\tau = 4$, and the value $m_\pi L \simeq 3.3$. Previously related HISQ studies on lattices with similar and comparable aspect ratios have found small finite-volume effects on bulk thermodynamic observables and pseudocritical temperatures within their quoted uncertainties. These results do provide useful guidance, but nevertheless a dedicated finite-volume study of these observables using UER would provide an important consistency check and a direct assessment of the associated systematic effects. A direct determination of finite-volume effects would require calculations at additional spatial volumes at fixed lattice spacing, over the full temperature range considered here. Such volumes with comparable statistics are not yet available for the present analysis. We therefore leave this systematic investigation of finite-volume effects using multiple spatial volumes for a future work. Regarding cutoff effects, the present study employs lattice with a single temporal extent, $N_\tau = 8$. Consequently, no continuum extrapolation is performed and residual discretization effects are not removed. A quantitative determination of these effects requires calculations at multiple values of N_τ. Previous HISQ studies indicate that cutoff effects in thermodynamic observables are reduced toward larger N_τ, while comparisons with continuum-extrapolated results suggest that discretization effects at $N_\tau = 8$ can lead to shifts of a few MeV in pseudocritical temperatures. Such comparisons provide an indication of the possible size of the effect but do not constitute a continuum extrapolation of the present calculation. The results presented here should therefore be regarded as $N_\tau = 8$ results. Dedicated calculations at finer lattice spacings are required for a controlled continuum determination.

A more precise determination of the curvature from the pseudocritical-line approach requires improved control over the definition of the pseudocritical temperature at finite $\hat{\mu}_B$, together with higher statistics and a systematic assessment of alternative pseudocritical estimators. The inclusion of higher-order terms in the parametrization of the crossover line also becomes important once the statistical precision is sufficient to constrain the lower-order terms. While the peak positions of $\hat{\chi}_T$ and $\hat{\chi}_C$ provide well-defined pseudocritical estimators at $\hat{\mu}_B = 0$, their interpretation at finite $\hat{\mu}_B$ is not uniquely established, the reasons of which have also been highlighted in this work. Further theoretical and numerical studies of their finite-density behavior are therefore needed. Future studies with higher-order cumulants, finer lattice spacings and multiple spatial volumes for analysing cutoff and finite-volume effects will enable controlled continuum and infinite-volume limit studies and provide a more quantitative assessment of the systematic uncertainties. Exploring the quark-mass dependence of these observables within the UER framework and approaching chiral limit also remains an important direction for future work. All relevant data for these computations depicted in the figures are in Ref. [22].

ACKNOWLEDGMENTS

I sincerely acknowledge useful discussions with Frithjof Karsch and Jishnu Goswami in this regard. This work has been supported by the Deutsche Forschungsgemeinschaft (DFG, German Research Foundation) Project No. 315477589-TRR 211. Computations and data analysis required for this work have been performed on the GPU cluster at Bielefeld University, Germany.

DATA AVAILABILITY

All relevant data for these computations depicted in the figures are in Ref. [22].

APPENDIX A: SINGULAR DEPENDENCE OF $\hat{\chi}_2^B$ AND ITS $\hat{\mu}_B$-DEPENDENT CORRECTION

Starting from the singular part of the free-energy density

$$\hat{f}_s^{\text{sing}} = -\hat{p}_s^{\text{sing}} = h_0 h^{1+1/\delta} f_f(z),$$

where $z = th^{-1/\beta\delta}$, the reduced temperature and symmetry-breaking field are given by

$$t = \frac{1}{t_0}\left(\frac{T - T_c}{T_c} + \kappa_2 \hat{\mu}_B^2 + \mathcal{O}(\hat{\mu}_B^4)\right), \qquad h = \frac{H}{h_0}.$$

Here, t_0 and h_0 are nonuniversal constants. The singular contribution to the second-order baryon susceptibility, $\hat{\chi}_2^B = \partial^2 \hat{p}/\partial \hat{\mu}_B^2$ can then be written as

$$\hat{\chi}_2^{B,s} = h_0\left[f_f''(z)\frac{4\kappa_2^2}{t_0^2} h^{-\alpha/(\beta\delta)}\hat{\mu}_B^2 + f_f'(z)\frac{2\kappa_2}{t_0} h^{(1-\alpha)/(\beta\delta)}\right], \tag{A1}$$

where the hyperscaling relation corresponding to three dimensional universality class, $2 - \alpha = \beta(1 + \delta)$ has been used. Factoring out the $\hat{\mu}_B$-independent prefactor, this takes the form

$$\hat{\chi}_2^{B,s} = A\left[f_f'(z) + \frac{2\kappa_2}{t_0} h_0^{1/(\beta\delta)} H^{-1/(\beta\delta)} \hat{\mu}_B^2 f_f''(z)\right], \tag{A2}$$

where $A = 2\kappa_2 h_0 h^{(1-\alpha)/\beta\delta}/t_0$ and $z_0 = h_0^{1/\beta\delta}/t_0$. Thus on simplifying the expressions, we find

$$\chi_2^{B,s} = A[f_f'(z) + 2\kappa_2 z_0 H^{-1/(\beta\delta)}\hat{\mu}_B^2 f_f''(z)]. \tag{A3}$$

On using the scaling estimate of $\kappa_2 = 0.02$, $H = 1/27$ and $z_0 = 1.42$ [21], where the critical exponents of the three-dimensional $O(2)$ universality class $\beta = 0.34864$, $\delta = 4.7798$ [23] are used, we find the coefficient of the correction term, $\hat{\mu}_B^2 f_f''(z)$ leading in $\mathcal{O}(\hat{\mu}_B^2)$ is

$$2\kappa_2 z_0 H^{-1/(\beta\delta)} \simeq 0.41,$$

and hence

$$\hat{\chi}_2^{B,s} = A[f_f'(z) + 0.41\,\hat{\mu}_B^2 f_f''(z)]. \tag{A4}$$

Taking a temperature derivative $\hat{\chi}_T^s = T\partial\hat{\chi}_2^s/\partial T$ and $\hat{\chi}_C^s = T_c\partial\hat{\chi}_2^s/\partial T$, the corresponding singular contributions to these thermal-derivative observables have the schematic form

$$\begin{aligned}\hat{\chi}_T^s &= A_T[f_f''(z) + 0.41\,\hat{\mu}_B^2 f_f'''(z)],\\ \hat{\chi}_C^s &= A_C[f_f''(z) + 0.41\,\hat{\mu}_B^2 f_f'''(z)],\end{aligned} \tag{A5}$$

where the overall positive proportionality factors, A_T and A_C differ for χ_T and χ_C.

A quantitative determination of this correction would require a reliable evaluation of the ratio $f_f'''(z)/f_f''(z)$ using the appropriate $O(2)$ scaling function in the range of z relevant for the present analysis. To estimate this range at $\hat{\mu}_B = 0$, we make use of $T_c = 143.7$ MeV, $H = 1/27$, and $z_0 = 1.42$. With $T_{\rm pc}^T = 160.2$ MeV and $T_{\rm pc}^C = 158.1$ MeV, one obtains

$$\begin{aligned}z_{\rm pc}^T &= z(\mathrm{T}_{\rm pc}^T) = z_0\frac{T_{\rm pc}^T - T_c}{T_c} H^{-1/(\beta\delta)} \simeq 1.17,\\ z_{\rm pc}^C &= z(\mathrm{T}_{\rm pc}^C) = z_0\frac{T_{\rm pc}^C - T_c}{T_c} H^{-1/(\beta\delta)} \simeq 1.02.\end{aligned} \tag{A6}$$

At $\hat{\mu}_B = 0.5$, using the same value $\kappa_2 = 0.02$, these become approximately

$$\begin{aligned}z_{\rm pc}^T &= z_0\left(\frac{T_{\rm pc}^T - T_c}{T_c} + \kappa_2\hat{\mu}_B^2\right) H^{-1/(\beta\delta)} \simeq 1.22,\\ z_{\rm pc}^C &= z_0\left(\frac{T_{\rm pc}^C - T_c}{T_c} + \kappa_2\hat{\mu}_B^2\right) H^{-1/(\beta\delta)} \simeq 1.07.\end{aligned} \tag{A7}$$

Thus close to the crossover temperature and with our working range of $\hat{\mu}_B$, $\hat{\mu}_B \in [0\!:\!0.5]$ considered here with $O(2)$ universal scaling relations, the relevant values of z remain in the range, $z \simeq 1$–1.2. We do not have such a controlled $O(2)$ determination here, due to which we refrain from assigning a numerical value to this ratio. Nevertheless, the explicit $\hat{\mu}_B^2$ prefactor provides a useful indication of the expected size of the correction. In particular, at the largest value considered in this work, $\hat{\mu}_B = 0.5$, this has a magnitude $\sim 0.41\,\hat{\mu}_B^2 = 0.1025 \sim 0.1$. Thus unless the ratio f_f'''/f_f'' becomes quite large in the relevant scaling region of z values given above in Eqs. (A6) and (A7), the higher-derivative contribution remains parametrically suppressed.

The available $O(4)$ scaling-function analysis in Ref. [24] indicates that f_f'''/f_f'' remains of moderate magnitude $\sim$0.3–0.5 in this region, with f_f'' and f_f''' having the same sign. While this observation cannot be directly interpreted as a quantitative estimate for the $O(2)$ theory, it provides a qualitative guidance that the quark-mass dependent higher-derivative term need not become large for $O(2)$ in particularly in the corresponding crossover region in case of physical quark masses, $H = 1/27$. This effect gets explicitly suppressed by the leading coefficient $0.41\hat{\mu}_B^2 \sim 0.1$ at $\hat{\mu}_B = \hat{\mu}_B^{\rm max} = 0.5$ and it is evident, that this suppression is more for lower $\hat{\mu}_B < 0.5$. Together with the smooth behavior expected for the universal scaling functions in the relevant z interval, this provides an indication that the finite-$\hat{\mu}_B$ modification of the thermal-derivative peak condition can be subleading for $\hat{\mu}_B \leq 0.5$.

This provides a justification for using the maxima of $\hat{\chi}_T$ and $\hat{\chi}_C$ as practical proxy estimators for the pseudocritical temperature, denoted by $T_{\rm pc}^T$ and $T_{\rm pc}^C$, respectively, in the small-$\hat{\mu}_B$ region considered here. We stress, however, that this argument is not a quantitative proof that the correction is negligible, since the required $O(2)$ ratio f_f'''/f_f'' has not been independently determined in the present work. At $\hat{\mu}_B = 0$, the derivative-based definitions provide natural estimators of the crossover location. At nonzero $\hat{\mu}_B$, however, additional derivatives of the scaling function enter the peak condition,

TABLE IV. Dependence of the pseudocritical temperatures T_{pc}^{T} and T_{pc}^{C} on the truncation order of the UER. Results obtained using the second- and fourth-order resummations are shown for several values of $\hat{\mu}_B$.

2nd order			4th order			Difference	
$\hat{\mu}_B$	T_{pc}^{T}	T_{pc}^{C}	$\hat{\mu}_B$	T_{pc}^{T}	T_{pc}^{C}	$\Delta_t T_{pc}^{T}$	$\Delta_t T_{pc}^{C}$
0.0	160.2(4)(3)	158.1(5)(3)	0.0	160.2(4)(3)	158.1(5)(3)	0.0	0.0
0.1	160.0(4)(3)	157.9(5)(4)	0.1	160.1(5)(3)	158.1(5)(3)	0.1	0.2
0.2	159.8(5)(4)	157.7(5)(4)	0.2	160.0(5)(2)	158.0(5)(1)	0.2	0.3
0.3	159.5(5)(3)	157.5(5)(3)	0.3	159.8(8)(1)	157.7(6)(0)	0.3	0.2
0.4	158.5(8)(7)	156.5(5)(5)	0.4	159.2(14)(0)	157.0(13)(0)	0.3	0.5
0.5	157.8(12)(8)	155.9(9)(5)	0.5	158.9(29)(1)	156.6(26)(0)	1.1	0.7

as illustrated above. Consequently, T_{pc}^{T} and T_{pc}^{C} should be regarded here as practical proxy or approximate definitions of the pseudocritical temperature rather than exact determinations of the finite-density pseudocritical line. Within the range $0 \leq \hat{\mu}_B \leq 0.5$, the explicit $\hat{\mu}_B^2$ suppression of the additional scaling contribution and the absence of any indication of a rapidly varying higher-derivative contribution in the relevant crossover region support this approximate interpretation. A more precise assessment of the systematic difference between these proxy definitions and the exact finite-density pseudocritical condition would require a dedicated analysis of the $O(2)$ free-energy scaling function and its higher derivatives, which is beyond the scope of present work.

APPENDIX B: DEPENDENCE OF PSEUDOCRITICAL TEMPERATURE ESTIMATE AND EXTRACTION PROCEDURE

In this appendix, we discuss the dependence of underlying systematics related to the determination of T_{pc}^{T} and T_{pc}^{C} on several factors: resummation order, functional form used for fitting data points, temperature interpolation in form of numerical resolution of intermediate points between a given range of temperature, the fitting range of temperature used casewise for cubic splines, and cubic and quartic global polynomials.

1. Resummation order

As a first assessment of systematic uncertainties, we investigate the dependence of the pseudocritical temperatures on the truncation order of the UER. As shown in Table IV, the pseudocritical temperatures obtained from the second- and fourth-order resummed susceptibilities are in good agreement over the range $0 \leq \hat{\mu}_B \leq 0.5$. For $\hat{\mu}_B \lesssim 0.3$, the differences between the two truncation orders are at most a few tenths of a MeV for both pseudocritical estimators. At the largest values of $\hat{\mu}_B$, the central values show a somewhat larger difference, reaching about 1.1 MeV for T_{pc}^{T} and 0.7 MeV for T_{pc}^{C} at $\hat{\mu}_B = 0.5$. These differences remain comparable to or smaller than the statistical uncertainties of the corresponding fourth-order determinations, and are therefore statistically consistent within the present precision.

The observed truncation-order dependence is consequently small compared with the overall uncertainties, although it becomes more visible at larger $\hat{\mu}_B$, where the statistical uncertainties also increase. We therefore use the fourth-order UER results for the remainder of the systematic analysis. The comparison with the second-order resummation provides an estimate of the sensitivity of the extracted pseudocritical temperatures to the truncation order.

2. Fit form or function dependence

We further investigate the dependence of the pseudocritical temperatures on the functional form used to represent the temperature dependence of the observables. Table V compares the results obtained using a cubic polynomial, a quartic polynomial, and a cubic spline over the range $135 \leq T \leq 172$ MeV. The three choices give mutually consistent values within the combined uncertainties. Relative to the cubic-spline result, the largest shifts are 0.5 MeV for T_{pc}^{T} and 0.6 MeV for T_{pc}^{C}, as observed from this Table V. These variations provide an estimate of the sensitivity of the pseudocritical temperature to the choice of interpolation, or the fitting form, given other parameters remain the same.

TABLE V. Dependence of the pseudocritical temperatures on the fitting or interpolation form for $135 \leq T \leq 172$ MeV. The cubic spline is used for the central analysis. The spread among the different fit forms involving cubic and quartic polynomials as global fits, is used to assess the associated systematic uncertainty.

Type of fit	T_{pc}^{T}	T_{pc}^{C}
Cubic polynomial	160.4(2)	158.3(1)
Quartic polynomial	160.7(2)	158.7(3)
Cubic spline	160.2(4)	158.1(6)

TABLE VI. Convergence of the pseudocritical temperatures with the number of fine points, N_{Fine}, used in the spline interpolation. The results are stable for $N_{Fine} \geq 200$, demonstrating that the numerical resolution of the interpolation does not contribute appreciably to the quoted uncertainties.

N_{Fine}	T^T_{pc}	T^C_{pc}
2	172.000(0)(0)	172.000 (0) (0)
20	160.153(416)(290)	158.134(480)(309)
200	160.163(428)(291)	158.108(533)(346)
1000	160.163(428)(291)	158.108(533)(346)
2000	160.163(428)(291)	158.108(533)(346)

3. Temperature interpolation

To verify that the determination of the pseudocritical temperatures is insensitive to the numerical resolution of the spline interpolation, we vary the number of fine points, N_{Fine}, used to locate the extremum of the interpolated functions for $\hat{\mu}_B = 0$. In this analysis outlined here, we restrict the range of temperature identical to the central analysis of this work, $[135:172]$ MeV, and use cubic spline interpolating fits for fitting the data points in this range, with 2000 bootstrap samples. As mentioned before, we outline this analysis here only for fourth order UER. The relevant results are summarized in Table VI. Both T^T_{pc} and T^C_{pc} show clear numerical convergence with increasing N_{Fine}. In particular, increasing N_{Fine} from 20 to 200 changes the central values by only 0.01 MeV for T^T_{pc} and 0.025 MeV for T^C_{pc}, while the results for $N_{Fine} = 200$, 1000 and 2000 are identical. Thus, the numerical resolution of the interpolation is negligible compared with the statistical and interpolation-range uncertainties. We therefore use $N_{Fine} = 2000$ in the subsequent analysis, involving cubic spline interpolating fitting to the respective data points.

The cubic spline is adopted as our central interpolation because it provides a smooth representation of the temperature dependence without imposing a specific global polynomial form. The observed fit-form dependence is included in our analysis of the systematic uncertainty associated with the temperature interpolation.

4. Fitting range of temperature

We investigate the dependence of the pseudocritical temperatures on the temperature interval used for the cubic-spline interpolation, and the relevant results are outlined in Table VII. First, we vary the lower bound T_{min} while keeping $T_{max} = 172$ MeV fixed. The resulting values of T^T_{pc} and T^C_{pc} show no significant systematic variation as the lower-temperature data points are removed. Similarly, fixing $T_{min} = 135$ MeV and varying the upper bound between 165 and 172 MeV results in essentially unchanged central values, with the statistical uncertainties increasing as the number of interpolation points is reduced. These results indicate that the determination of the pseudocritical temperatures is stable against reasonable variations of the interpolation range.

For comparison, extending the interpolation interval to $T_{max} = 180$ MeV leads to substantially larger uncertainties and a noticeable shift in the extracted central values. This behavior reflects the increased sensitivity of the spline interpolation to the high-temperature boundary, where the available data provide weaker constraints. We therefore regard the 135–180 MeV result as an indication of boundary sensitivity rather than as evidence for a systematic shift of the pseudocritical temperature.

We also examine the dependence of the pseudocritical temperatures on the fit range using global cubic and quartic polynomial forms. As depicted by Table VIII for the cubic polynomial, the results remain relatively stable when the

TABLE VII. Table showing dependence of T_{pc} obtained from the peak locations of $\hat{\chi}_x, x \equiv T, C$, on the temperature interval $[T_{min}, T_{max}]$ used for the interpolation. The first group probes broader interpolation intervals, the second varies the lower boundary at fixed $T_{max} = 172$ MeV, and the third varies the upper boundary at fixed $T_{min} = 135$ MeV.

Cubic Spline				
T_{min}	T_{max}	T^T_{pc}	T^C_{pc}	# Data points
130.0	172.0	160.4(7)(4)	158.4(8)(7)	8
135.0	172.0	160.2(4)(3)	158.1(5)(3)	7
145.0	172.0	160.2(3)(2)	158.2(4)(2)	6
150.0	172.0	160.0(3)(0)	157.6(5)(0)	5
135.0	180.0	157.4(80)(41)	155.3(78)(41)	8
135.0	172.0	160.2(4)(3)	158.1(5)(3)	7
135.0	170.0	160.1(4)(3)	158.1(6)(4)	6
135.0	165.0	160.0(12)(11)	158.2 (8)(7)	5

lower boundary is varied from 135 to 145 MeV at fixed $T_{\max} = 172$ MeV, while a larger variation is observed when the fit is extended to $T_{\min} = 130$ MeV or restricted to $T_{\min} = 150$ MeV. At fixed $T_{\min} = 135$ MeV, the 135–170 and 135–172 MeV fits give consistent results, whereas the narrower 135–165 MeV interval leads to substantially larger uncertainties. The quartic polynomial exhibits a stronger dependence on the fit range. In particular, reducing the number of data points leads to increased variation of the extracted pseudocritical temperatures and larger uncertainties, and the quartic fit does not provide a determination of T_{pc}^{C} for the 150–172 MeV interval. The 135–165 MeV quartic fit also shows a substantial shift relative to the broader fit ranges. These observations indicate that higher-order global polynomial forms become increasingly sensitive to the available fit interval when the number of data points is small.

TABLE VIII. Dependence of the pseudocritical temperatures, obtained from the peak locations of $\hat{\chi}_x$, $x \equiv T$, C, on the temperature interval $[T_{\min}, T_{\max}]$ used in the cubic and quartic polynomial fits. The first group varies the lower boundary at fixed $T_{\max} = 172$ MeV, while the second varies the upper boundary at fixed $T_{\min} = 135$ MeV.

Cubic polynomial				Quartic polynomial			
$T_{\min}$	$T_{\max}$	T_{pc}^{T}	T_{pc}^{C}	$T_{\min}$	$T_{\max}$	T_{pc}^{T}	T_{pc}^{C}
130.0	172.0	161.4(2)	158.8(1)	130.0	172.0	161.0(1)	159.3(1)
135.0	172.0	160.4(2)	158.3(1)	135.0	172.0	160.7(2)	158.7(3)
145.0	172.0	160.4(1)	158.4(1)	145.0	172.0	159.6(4)	157.6(4)
150.0	172.0	160.0(3)	157.6(5)	150.0	172.0	160.2(8)	Nan
135.0	180.0	160.70(6)	158.50(5)	135.0	180.0	160.6(2)	158.4(2)
135.0	172.0	160.4(2)	158.3(1)	135.0	172.0	160.7(2)	158.7(3)
135.0	170.0	160.6(4)	158.4(3)	135.0	170.0	160.2(3)	158.7(2)
135.0	165.0	161.8 (10)	159.4(8)	135.0	165.0	158.3(5)	157.4(3)

[1] D. Bollweg, J. Goswami, O. Kaczmarek, F. Karsch, S. Mukherjee, P. Petreczky, C. Schmidt, and P. Scior, (HotQCD), Taylor expansions and Padé approximants for cumulants of conserved charge fluctuations at nonvanishing chemical potentials, Phys. Rev. D **105**, 074511 (2022).

[2] D. Bollweg, D. A. Clarke, J. Goswami, O. Kaczmarek, F. Karsch, S. Mukherjee, P. Petreczky, C. Schmidt, and S. Sharma, (HotQCD), Equation of state and speed of sound of $(2+1)$-flavor QCD in strangeness-neutral matter at nonvanishing net baryon-number density, Phys. Rev. D **108**, 014510 (2023).

[3] C. R. Allton, S. Ejiri, S. J. Hands, O. Kaczmarek, F. Karsch, E. Laermann, C. Schmidt, and L. Scorzato, The QCD thermal phase transition in the presence of a small chemical potential, Phys. Rev. D **66**, 074507 (2002).

[4] C. R. Allton, M. Doring, S. Ejiri, S. J. Hands, O. Kaczmarek, F. Karsch, E. Laermann, and K. Redlich, Thermodynamics of two flavor QCD to sixth order in quark chemical potential, Phys. Rev. D **71**, 054508 (2005).

[5] A. Bazavov *et al.* (HotQCD Collaboration), Equation of state in $(2+1)$-flavor QCD, Phys. Rev. D **90**, 094503 (2014).

[6] A. Bazavov *et al.* (HotQCD Collaboration), Chiral crossover in QCD at zero and nonzero chemical potentials, Phys. Lett. B **795**, 15 (2019).

[7] S. Borsanyi, Z. Fodor, J. N. Guenther, R. Kara, S. D. Katz, P. Parotto, A. Pasztor, C. Ratti, and K. K. Szabo, QCD crossover at finite chemical potential from lattice simulations, Phys. Rev. Lett. **125**, 052001 (2020).

[8] S. Gupta, Lattice QCD with chemical potential: Evading the fermion-sign problem, Pramana **63**, 1211 (2004).

[9] P. de Forcrand and O. Philipsen, The QCD phase diagram for small densities from imaginary chemical potential, Nucl. Phys. **B642**, 290 (2002).

[10] S. Mitra, P. Hegde, and C. Schmidt, New way to resum the lattice QCD Taylor series equation of state at finite chemical potential, Phys. Rev. D **106**, 034504 (2022).

[11] S. Mitra and P. Hegde, QCD equation of state at finite chemical potential from an unbiased exponential resummation of the lattice QCD Taylor series, Phys. Rev. D **108**, 034502 (2023).

[12] S. Mitra, Exponential resummation of QCD at finite chemical potential, Ph.D. thesis, Indian Institute of Science Bangalore, Centre for High Energy Physics, India, Bangalore, Indian Inst. Sci., 2023, arXiv:2307.05751.

[13] S. Mitra, P. Hegde, and C. Schmidt, A new way to resum Lattice QCD equation of state at finite chemical potential, Proc. Sci. LATTICE2022 (**2023**) 153 [arXiv:2209.07241].
[14] S. Mitra, Determination of lattice QCD equation of state at a finite chemical potential, Springer Proc. Phys. **304**, 209 (2024).
[15] S. Mitra, Estimates of Lee-Yang zeros and a possible critical point on the pion condensate boundary in the QCD isospin phase diagram using an unbiased exponential resummation on the lattice, Phys. Rev. D **112**, 014511 (2025).
[16] K. Symanzik, Continuum limit and improved action in lattice theories. 1. Principles and φ^4 theory, Nucl. Phys. **B226**, 187 (1983).
[17] S. Mitra, F. Karsch, and S. Sharma, Towards a parameter-free determination of critical exponents and chiral phase transition temperature in QCD, Proc. Sci. LATTICE2024 (**2025**) 187 [arXiv:2411.15988].
[18] S. Mitra and F. Karsch, Towards a parameter-free analysis of the QCD chiral phase transition and its universal critical behavior, Springer Proc. Phys. **432**, 781 (2026).
[19] S. Mitra and F. Karsch, Finite-volume analysis and universal scaling signatures near the chiral phase transition in $(2+1)$-flavor QCD, EPJ Web Conf. **364**, 15004 (2026).
[20] S. Mitra, J. Goswami, and F. Karsch, Universal and non-universal finite-volume effects in the vicinity of chiral phase transition in $(2+1)$-flavor QCD, Proc. Sci. LATTICE2025 (**2026**) 118 [arXiv:2602.23118].
[21] H. T. Ding, O. Kaczmarek, F. Karsch, P. Petreczky, M. Sarkar, C. Schmidt, and S. Sharma, Curvature of the chiral phase transition line from the magnetic equation of state of $(2+1)$-flavor QCD, Phys. Rev. D **109**, 114516 (2024).
[22] S. Mitra, Numerical data for "The QCD crossover temperature and curvature coefficient from unbiased exponential resummation at physical quark masses in $(2+1)$-flavor lattice QCD," 10.5281/zenodo.23356418 (2026).
[23] F. Karsch, M. Neumann, and M. Sarkar, Scaling functions of the three-dimensional Z(2), O(2), and O(4) models and their finite-size dependence in an external field, Phys. Rev. D **108**, 014505 (2023).
[24] C. Schmidt (BNL-Bielefeld-CCNU Collaboration), Exploring the QCD phase diagram with conserved charge fluctuations, Proc. Sci. LATTICE2014 (**2015**) 186.